CRS-STACK-BASED SEISMIC IMAGING AS A CASE STUDY FOR BASIN REEVALUATION

Z. Heilmann, L. Leite, and A. Gomes

email: *Zeno.Heilmann@gpi.uni-karlsruhe.de*

keywords: *CRS-stack-based imaging, kinematic wavefield attributes, surface topography, residual static corrections, tomographic inversion, depth migration*

ABSTRACT

In this case study we are giving attention to the seismic processing and interpretation of a land data set from the Takutu basin, Brazil. This aims at establishing a new seismic imaging workflow well suited to the specific problems of land data processing, namely, sparse data, complex geological structures, and complicated near surface conditions. The presented extension of CRS-stack-based time-to-depth imaging supports arbitrary top-surface topography. We applied the following processing steps: CRS stack, residual static correction, determination of a macrovelocity model via tomographic inversion, and Kirchhoff pre- and poststack depth migration. Our CRS stack implementation combines two different approaches of topography handling to a cascaded processing strategy that demands very little additional effort. After initial values of the CRS attributes are determined for a smoothly curved measurement surface, the final CRS stack and also the CRS-stack-based residual static correction are applied to the original prestack data, considering the true source and receiver elevations. This is very important to achieve physical meaningful CRS attributes. Conventional elevation statics that assume every ray to emerge vertically deteriorate the CRS attributes, similar as in case of the stacking velocity. After the CRS stack is completed, we utilize the extracted emergence angles to relate the stacked zero-offset section, the CRS attribute sections and the quality control sections to a chosen planar reference level. This redatuming procedure removes the influence of the rough measurement surface from the CRS stack results and provides standardized input for interpretation, tomographic inversion, and poststack depth migration. As a final step, we applied a prestack depth migration from topography using the prestack data after residual static correction.

INTRODUCTION

In the current situation of rapidly growing demand in oil and gas, on-shore exploration, even under difficult conditions, becomes again more and more important. Unfortunately, rough top-surface topography and a strongly varying weathering layer often result in poor data quality, which makes conventional data processing very difficult to apply. Under such circumstances, where simple model assumptions may fail, it is of particular importance to extract as much information as possible directly from the measured data. Fortunately, the ongoing increase in available computing power makes so-called data-driven approaches (see, e. g., Hubral, 1999) feasible which, thus, have increasingly gained in relevance during the last years. The Common-Reflection-Surface (CRS) stack (see, e. g., Mann, 2002) is one of these promising methods. Besides an improved zero-offset simulation, its decisive advantage over conventional methods is that for every zero-offset sample several so-called kinematic wavefield attributes are obtained as a by-product of the data-driven stacking process. As will be shown, they can be applied both, to improve the stack itself and to support subsequent processing steps. Using these *CRS attributes*, an advanced data-processing workflow can be established leading from time to depth domain, covering a broad range of seismic reflection imaging issues in a consistent manner. The major steps of this workflow are displayed in Figure 1.

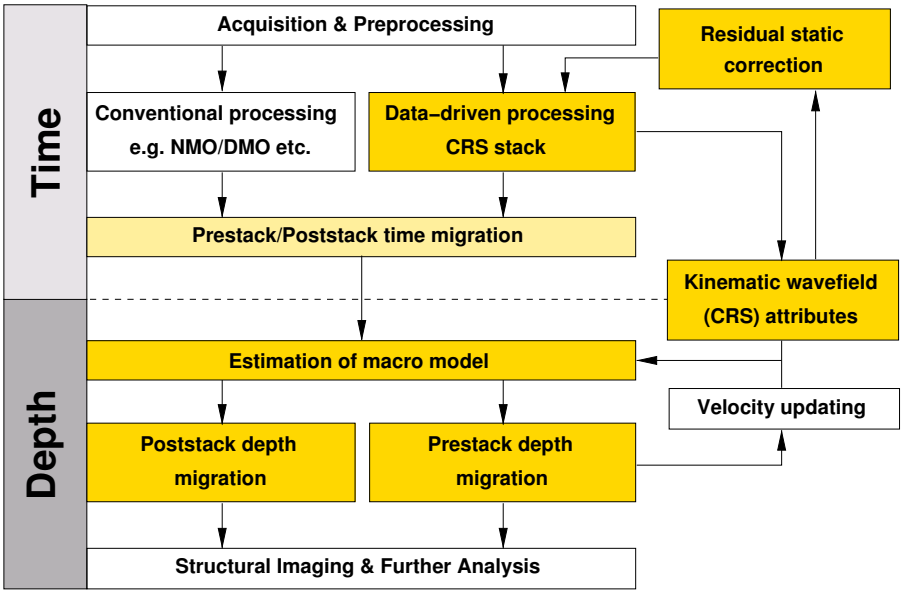

Figure 1: Major steps of seismic-reflection data processing in time and depth domain. Imaging procedures that can be incorporated in the CRS-stack-based imaging workflow are highlighted in yellow.

TAKUTU DATASET

The Takutu dataset used in the case study was acquired by PETROBRAS (Takutu Basin, Rondônia, Brazil) for petroleum exploration. The data is free for use on university research and it was obtained from ANP (Agência Nacional do Petróleo). The goal here is to support academic projects that can deal with basin reevaluation based on seismic reprocessing. The software used is non-commercial, developed in the spirit of continuous cooperation between the Geophysics Department of the Federal University of Pará (Brazil) and the Wave Inversion Technology (WIT) Consortium of the University of Karlsruhe, Germany. This data set is offered in the form of non-processed field records, therefore a complete preprocessing stage was necessary.

Following the description by Eiras and Kinoshita (1990), the Takutu basin is classified as a Mesozoic intracontinental rift, oriented NE-SW, with approximately 300 km length and 40 km width. It was developed in the central part of the Guyana shield, and it is located at the border between Brazil and Guyana. The rift is filled with sediments ranging from the Jurassic to the Quaternary, and composed of two asymmetrical half-grabens: The SW part dips southeasterly and the NE part dips northwesterly.

The structural scenario of the Takutu basin features horsts, grabens, anticlines, synclines, flower structures, and dip inversions (rollovers). Transcurrent faulting is considered to have reactivated local features that were developed in the rift stage (Figure 2).

The stratigraphic scenario of the Takutu basin is divided into four depositional sequences that reflect the geological evolution of the area (Figures 3, 4 and 5). The first basal sequence is represented by the volcanic Apoteri formation and by the shaly Manari formation, both related to the pre-rift phase. The second sequence is represented by the evaporitic Pirara formation, and relates to the stage of maximum stretching in the rift phase. The third sequence is represented by the sands and conglomerates of the Takutu and Tucano formations, and is interpreted to correspond to the continuous decrease in stretching. The fourth sequence is represented by the lateritic and alluvium of the Boa Vista and North Savannas formations.

Continuing with Eiras and Kinoshita (1990), the conclusions for the model of the Takutu basin were formally based on the interpretation of the conventionally processed seismic data, seismic reprocessing, seismic stratigraphy, surface geology, drilled wells, geochronology and geochemistry. Several structural styles were considered for the basin in focus, and the most attractive were deltaic fan-shaped, compressional inversions, internal horst highs, and dip reversals. Our intention at this moment is not yet to trace new evidences for the structural scenario for the Takutu basin; this may follow with the course of the studies with

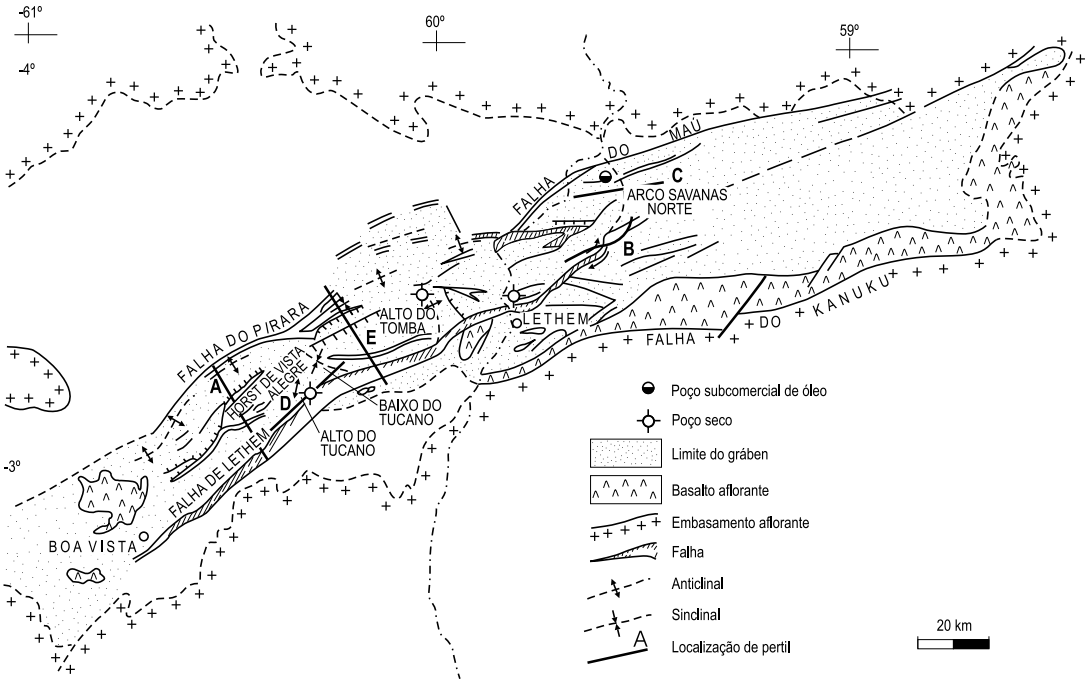

Figure 2: Structural map of Takutu graben redrew from Eiras and Kinoshita (1990) showing the directions of the seismic lines.

more systematically processed data completing at least a full block for a proper geological interpretation. Among the processed lines, the selected line for this case study was the one numbered 204-239. It has the following survey information: date of acquisition 1986; direction NW-SE; length of 31.5 km; 631 shot points; 4 ms of time sampling interval; 50 m spacing of shot points and stations; charges of 0.9 kg at 2 m depth distributed as L-3x2/25 m. The array distribution from left to right starts with a part right-unilateral 0-48; the second part is split-spread symmetrical 48-48; the third part is split-spread asymmetrical 76-20; and the fourth part is a left-unilateral 76-0. Unfortunately, the data quality from 20 km to 31.5 km distance is very bad so that hardly any continuous reflection event could be imaged. Consequently, we had to limit the target area for this case study to the range between 0-20 km.

The preprocessing steps were performed with the CWP/SU package of the Colorado School of Mines (Cohen and Stockwell, 2000), whose data format is also used in the CRS code. Similar procedures should be carried out for all the lines of the two seismic blocks (numbered 50 and 204) of the Takutu graben. The tasks consisted of 3 main parts: (1) Geometry setting; (2) Muting of bad traces (3) F and F-K filtering (4) Trace balancing.

As a first observation about the original Takutu seismic land-data, the line 204-239 has many noisy sections. For this reason, several shot and receiver gathers were initially completely muted. Afterward, as a result of visual analysis of all shot gathers, again several single traces had to be zeroed due to the high noise level like spikes and sensor wandering. As a second observation, several band-pass filters with polygonal form were experimented, and the decision was for adopting the case with corners 8-10-35-45 Hz. The F-K velocity dependent filter was used to further emphasize the cutting of surface waves and critically refracted waves. The decision for adopting the filter parameters was based on the trace gathers analysis through the spectrum and preliminary stack results, reinforcing the importance of the preprocessing stage on the CRS stack results. Also, it should be mentioned that no deconvolution was carried out on this data.

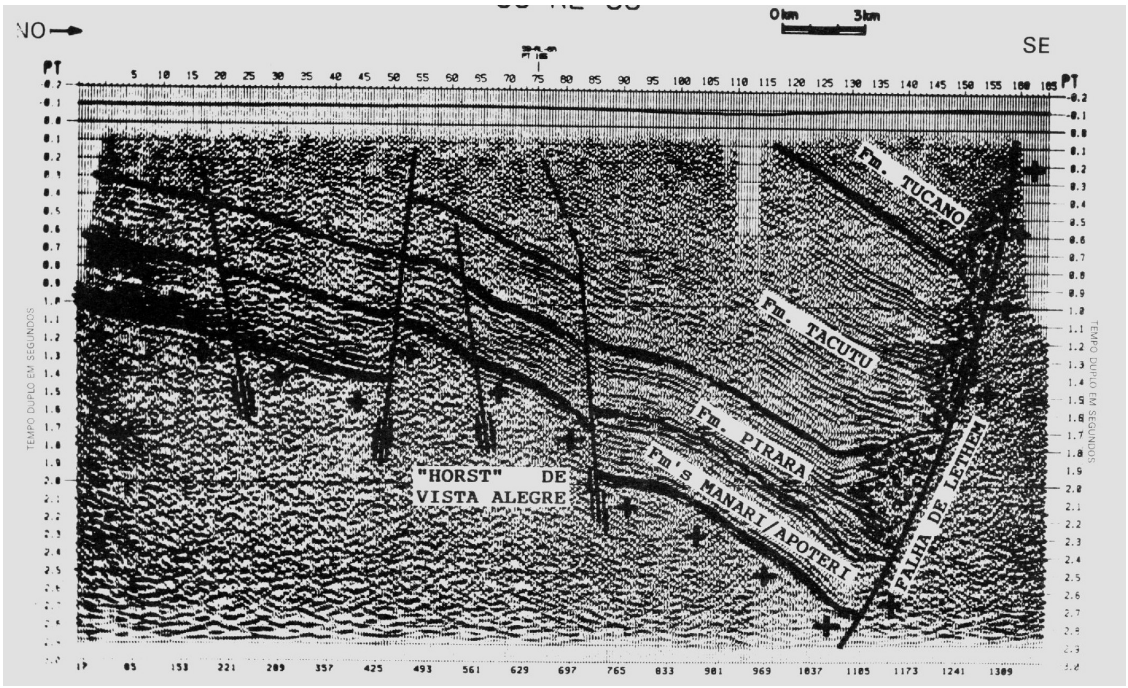

Figure 3: Seismic section A from Eiras and Kinoshita (1990) with aspects of geological interpretation for Takutu graben.

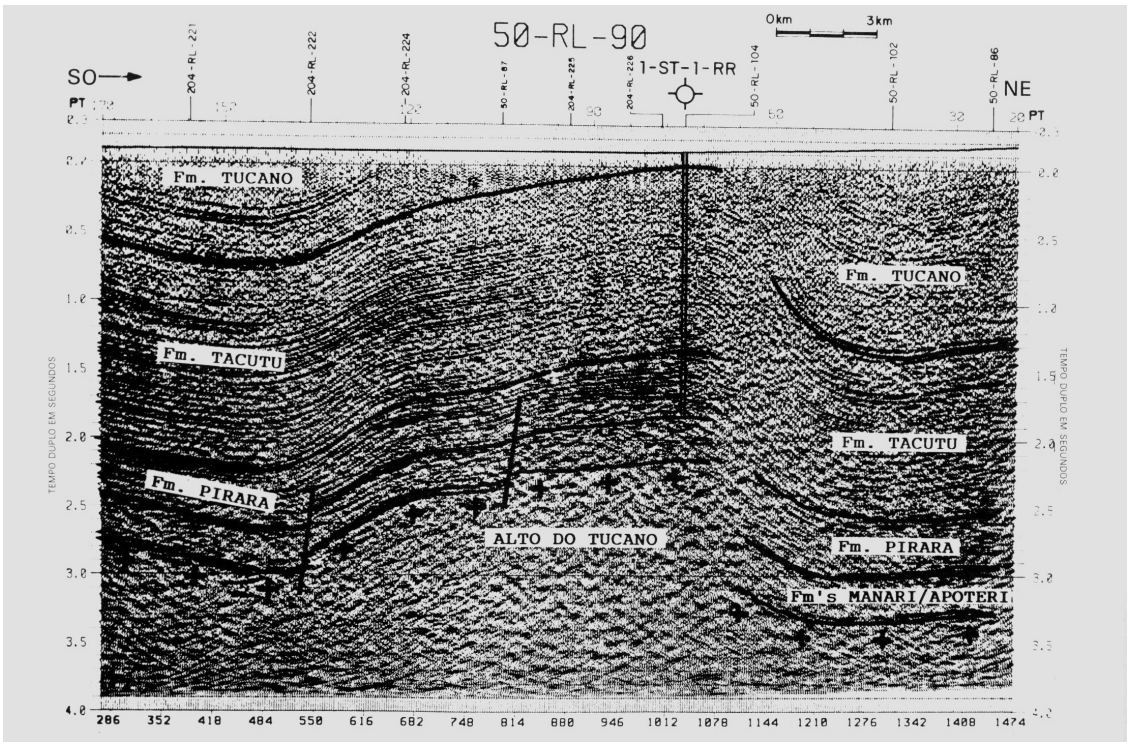

Figure 4: Seismic section D from Eiras and Kinoshita (1990) with aspects of geological interpretation for Takutu graben.

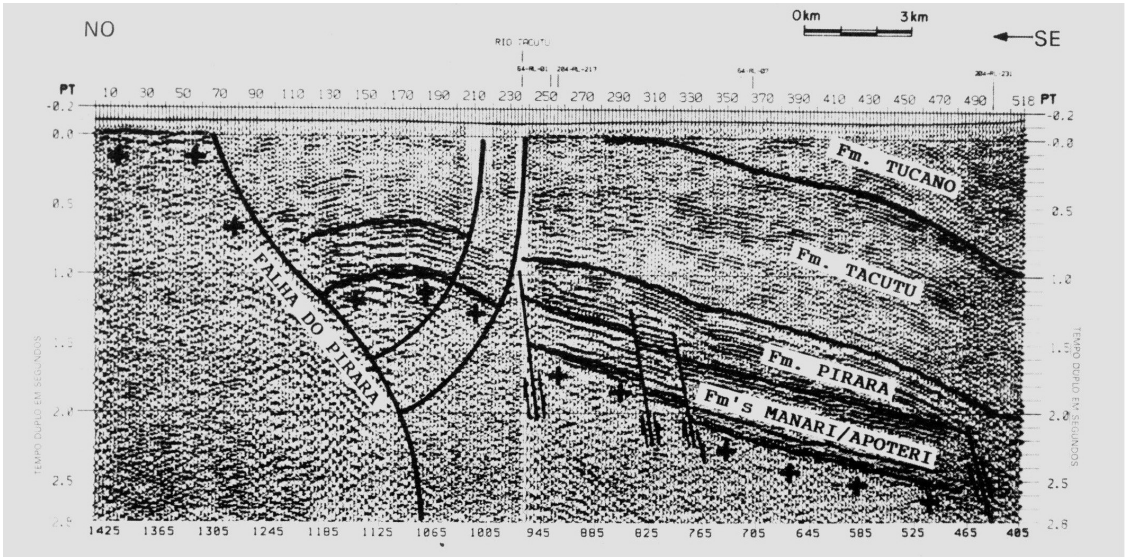

Figure 5: Seismic section E from Eiras and Kinoshita (1990) with aspects of geological interpretation for Takutu graben.

CRS STACK FOR TOPOGRAPHY

The simulation of stacked ZO sections is routinely applied to enhance the signal-to-noise ratio and reduce the amount of seismic data for further processing. A conventional approach to achieve this goal is the application of normal moveout (NMO) and dip moveout (DMO) corrections to the multicoverage dataset followed by a subsequent stack along the offset axis, usually denoted as NMO/DMO/stack (e. g., Yilmaz, 2001). The CRS stack (e. g., Müller, 1999; Jäger et al., 2001; Mann, 2002) is a powerful alternative to this conventional approach that can be seen as a generalized multi-dimensional high-density stacking-velocity analysis tool. It has been reported by several case studies, e.g. Gierse et al. (2003), that the CRS stack produces reliable stack sections with high resolution and signal-to-noise ratio. As mentioned before a set of physically interpretable stacking parameters is determined as a result of the data-driven stacking process. These kinematic wavefield attributes obtained by the CRS stack are important because they can be applied to solve a number of dynamic and kinematic problems (see Figure 1). So far, CRS-stack based seismic imaging was limited to data acquired on a planar measurement surface or at least to data for which a planar measurement surface had been simulated by elevation statics. However, conventional elevation statics may introduce a certain error to the stack and—even worse—to the CRS attribute sections, as a vertical emergence of all rays has to be assumed. In case of rough top-surface topography this error might significantly deteriorate the results of the CRS stack and of all processing steps based on it. Therefore, we extended the existing implementations of CRS stack and CRS-stack-based residual static correction to consider the true source and receiver elevations (Heilmann, 2003; von Steht, 2004; Koglin, 2005).

In recent years, two different CRS stacking operators that consider the top-surface topography have been developed at Karlsruhe University [see Appendix A]. Chira et al. (2001) assumed a smoothly curved measurement surface for which the elevation of all source and receiver points contributing to a single stacking process can be approximated by a parabola. This approach is attractive from the computational point of view as it allows to adopt most parts of the conventional CRS stack implementation. In particular, the pragmatic CRS-attribute search strategy using three one-parameter searches to determine the optimal stacking operator can be maintained. However, small elevation statics are still required in order to transfer the real data to the chosen smoothly curved measurement surface. Zhang (2003) presented a very general CRS stacking operator that directly considers the true elevation of every source and receiver. This approach demands far more computational effort, as at least two of the three CRS attributes have to be searched for simultaneously due to the higher complexity of the stacking operator. On the other hand, no elevation

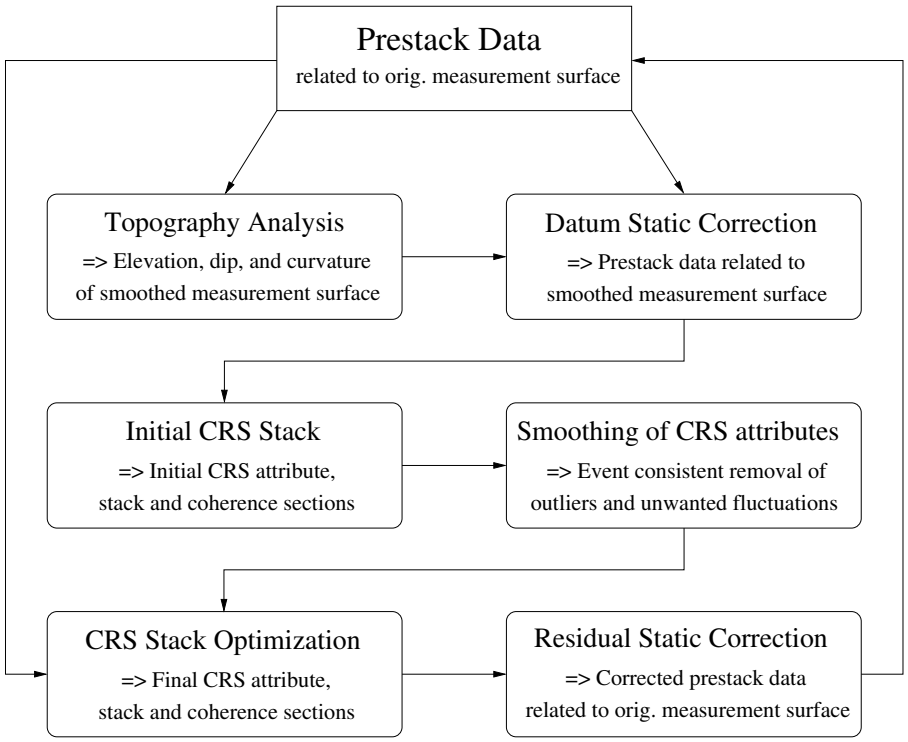

Figure 6: *Cascaded processing scheme for topography handling in CRS stack and CRS stack based residual static correction*

statics are required and the elevations of the emergence points of the simulated zero-offset rays can be chosen—within certain limits—arbitrarily. A similar approach based on the methology of *Multifocusing* was presented in Gurevich et al. (2001).
Following the idea of a step-by-step refinement, we chose an implementation that combines both methods of topography handling mentioned above to a cascaded processing strategy. Doing this, most of the specific disadvantages of the single approaches can be compensated without loosing their individual benefits. In a final step, we relate the CRS stack results to a planar reference datum close to the actual measurement surface. By this redatuming procedure a seamless transition to the tomographic inversion and other succeeding processing steps is provided. A flowchart of this pragmatic strategy is depicted in Figure 6.

Initial CRS stack

As shown by Heilmann (2003), the CRS traveltime operator for smoothly curved topography is well suited to determine initial values of the CRS attributes. Therefore, the global search is splitted into three one-parameter searches. Each parameter is determined in a specific 2D subset of the 3D data volume. In order to apply the CRS traveltime operator for a smoothly curved measurement surface to our data set we have (1) to find an appropriate smooth reference surface, (2) to determine the local dip and curvature in every CMP location, and (3) to apply datum static corrections that relate the prestack data to this surface.
For this purpose, it is necessary to consider that, in general, the larger the scale of the smoothing the larger the elevation static correction which has to be applied. Nevertheless, the surface has to be smooth enough such that for every single stacking process the elevations of all contributing sources and receivers can be well approximated by a parabola. To control the degree of smoothing, a smoothing window was introduced. As a rule of thumb, its size should be in the range of the maximum offset aperture used for the wavefield attribute search and the stacking procedure. A comparison between the original measurement surface and its smoothed counterpart can be found in Figure 7.

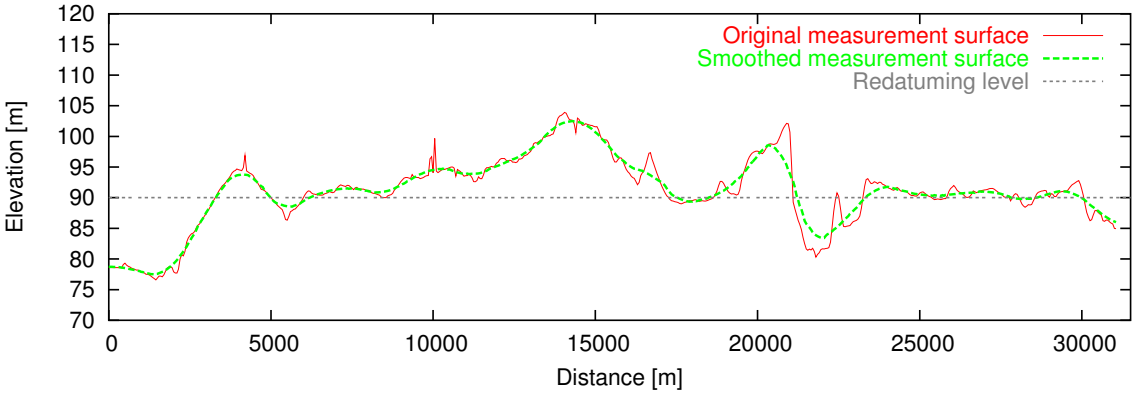

Figure 7: *Comparison between original and smoothed measurement surface. The horizontal redatuming level at $z = 90$ m is also displayed.*

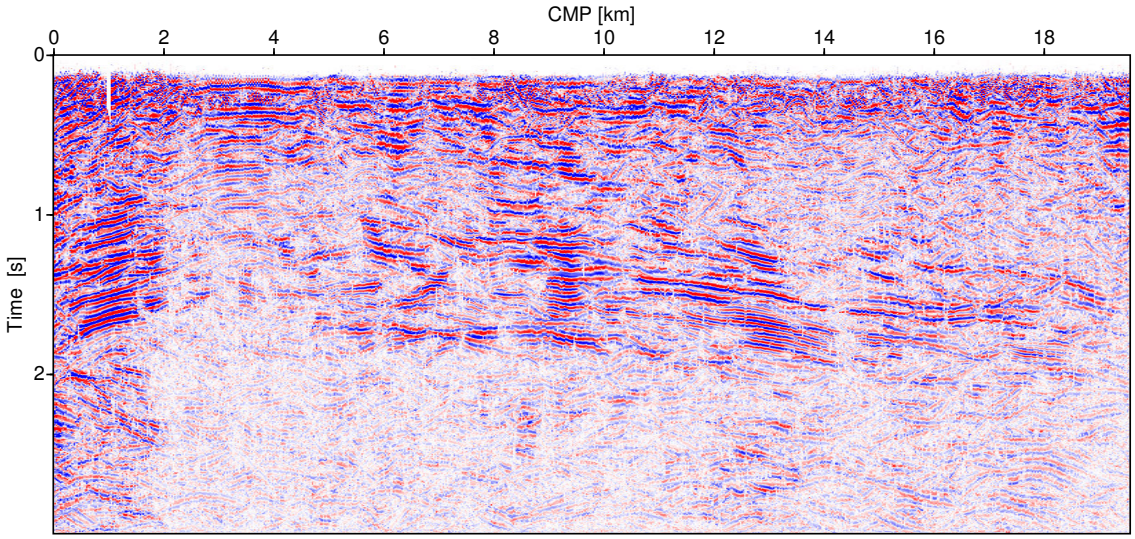

Figure 8: ZO section achieved by initial CRS stack considering a smooth curved measurement surface

The datum static correction for every source and receiver location is calculated from the near-surface velocity and the differences in elevation of the true source and receiver points and their vertical projections onto the smoothed surface. In this specific case we can assume a laterally constant near-surface velocity, i. e. the replacement velocity used in the preprocessing. For every zero-offset sample the kinematic wavefield attributes K_{NIP}, K_{N}, and β_0 are determined by means of three one-parameter searches. Thus, an individual stacking operator (13) is defined for every sample of the zero-offset section. The summation process is performed within a user-defined aperture or within an aperture that accounts for the size of the projected first Fresnel zone for offset zero. The latter can be estimated from the CRS attributes by comparing the approximated traveltime of the actual reflection event with the approximated traveltime of its associated diffraction event (characterized by the property $K_{\mathrm{N}} \rightarrow K_{\mathrm{NIP}}$). The locations where the zero-offset traveltimes of these events differ by the temporal wavelet length define the extension of the considered projected first Fresnel zone and, thus, the optimum aperture to apply the attribute search and the stack. The initial CRS stack result achieved in this step is depicted in Figure 8.

Event-consistent smoothing

At this stage, event-consistent smoothing of the initial attributes can be helpful to remove fluctuations and outliers. The latter are mainly caused by the limitations of the utilized three-times-one parameter search

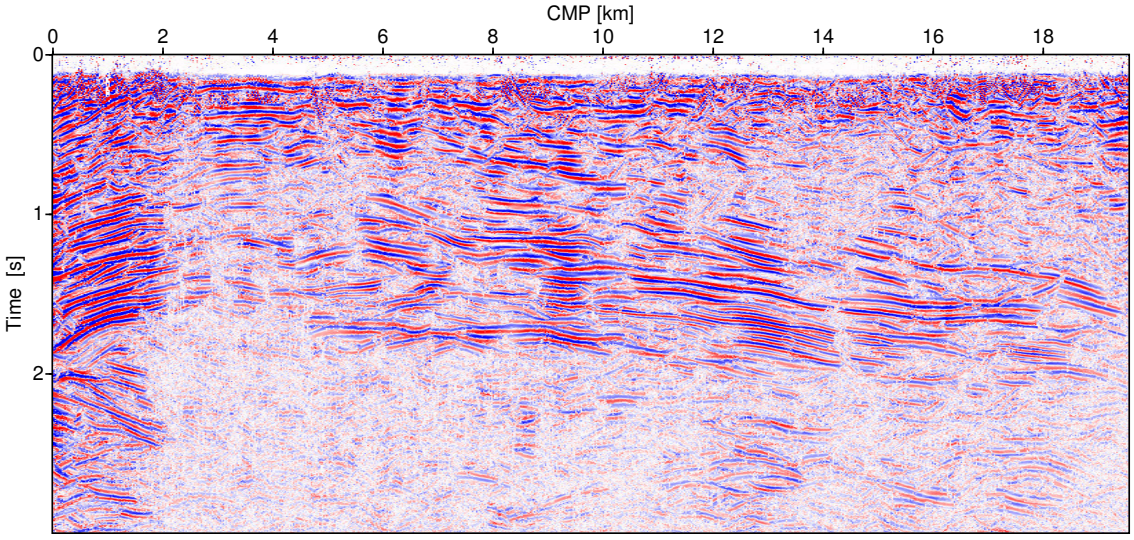

Figure 9: ZO section after event-consistent smoothing and three-parameter optimization.

strategy. The smoothing algorithm itself is based on the combined application of mean and median filtering in volumes aligned with reflection events. The information about slopes of events in the time domain is readily available from the CRS attributes themselves and allows to avoid the mixing of intersecting events. By this means, the smoothing algorithm can be designed in an event-consistent manner. This process does not imply any loss of information about the parameterized reflection events (see, e. g., Mann and Duveneck, 2004). Thus, even in case of conflicting dip situations, it often provides significantly improved input for the subsequent optimization. In case of complex near-surface conditions which often lead to a strongly variable data quality along the line, this intermediate processing step was especially successful.

Three-parameter optimization considering the true topography

An important feature of the CRS traveltime operator for arbitrary topography (2) is that the elevation of the emergence point X_0 of each zero-offset ray to be simulated can be chosen arbitrarily. This property provides the link to the initial results determined under the assumption of a smoothly curved measurement surface. Since the latter are related to a fictitious smoothly curved measurement surface we choose this surface also as reference level for the optimization. By this means, the zero-offset rays to be simulated are identical in both cases. Therefore, it can be expected that the CRS attributes obtained in the previous step are close to their optimum values and, thus, well suited as initial values for a local three-parameter optimization using equation (2). The objective function to be maximized is, as in case of the one-parameter searches, the semblance (Neidell and Taner, 1971), a measure of the coherence of the prestack data along the stacking operator. Particularly in noisy areas, a significantly increased continuity of the reflection events can be expected.
To confine the spatial extent of the stacking operator, the projected first Fresnel zone is taken into account. Both, the local optimization and the stacking itself are applied to the original, i. e., uncorrected, data using the CRS traveltime operator for arbitrary topography. Consequently, any inaccuracies of the initial stack and especially of the initial attributes caused by the elevation statics should be compensated. Nevertheless, stack and attribute sections are still related to the floating datum corresponding to the smooth reference surface. The resulting stack section after event-consistent smoothing of the CRS attributes and three-parameter optimization is depicted in Figure 9.

Redatuming

Floating datum sections are no appropriate input for interpretation or further processing. Therefore, we implemented a redatuming procedure that relates the CRS stack results to a fictitious horizontal measure-

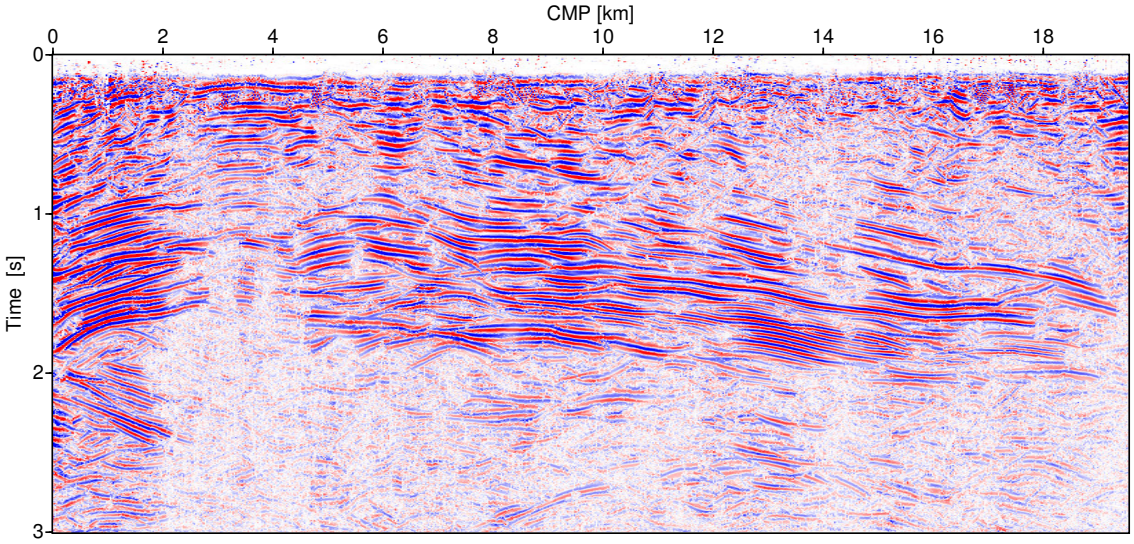

Figure 10: ZO section after two iterations of residual static correction and redatuming to horizontal reference level at $z = 90m$

ment surface close to the smoothly curved reference level (see Figure 7). Due to the fact that the emergence angle of every simulated zero-offset ray is known, it is easy to continue them to a constant reference level—especially, if the replacement velocity v_r between the smoothly curved and the planar surface is chosen to equal the near-surface velocity v_0 [see Appendix B]. In this case no refraction has to be considered when crossing the smoothly curved reference level.

RESIDUAL STATIC CORRECTION

The CRS-stack-based residual static correction methodology (Koglin, 2005) is an iterative process close to the super-trace cross-correlation method by Ronen and Claerbout (1985). However, the cross correlations are performed within CRS supergathers of moveout corrected prestack traces instead of being confined to single CMP, common-shot, or common-receiver gathers. The moveout correction makes use of the previously obtained CRS attributes and considers the true source and receiver elevations. Thus, elevation static correction can be omitted that may introduce, in certain cases, non surface-consistent errors of the same scale as the searched-for residual statics.

Due to the spatial extent of the CRS operator, the CRS supergathers contain many neighboring CMP gathers but with different moveout corrections depending on the current zero-offset location. Thus, the cross correlations of the stacked trace (here used as pilot trace) and the moveout corrected prestack traces are summed up for each shot and receiver location. This summation is performed for all CRS supergathers contained in the specified target zone. After all cross correlations are summed up, the searched-for residual time shifts are expected to be associated with maxima in the cross correlation stacks. Finally, the estimated time shifts are used to correct the prestack traces and the next iteration of residual static correction can be started. Now, the entire CRS stack process is repeated using the corrected prestack data set. The optimized CRS stack section after two iterations of residual static correction and redatuming is depicted in Figure 10. It can be observed that besides an strongly improved resolution and event continuity also the small scale undulations of the reflection events are mostly removed.

TOMOGRAPHIC INVERSION

In order to obtain a depth image from the time-domain pre- and/or poststack data, a macrovelocity model needs to be estimated, which is one of the crucial steps in seismic data processing. Fortunately, such a model can be obtained directly from the CRS stack results: the attributes R_{NIP} and β_0 related to the hypothetical normal-incidence-point (NIP) wave at a given ZO location describe the approximate multi-

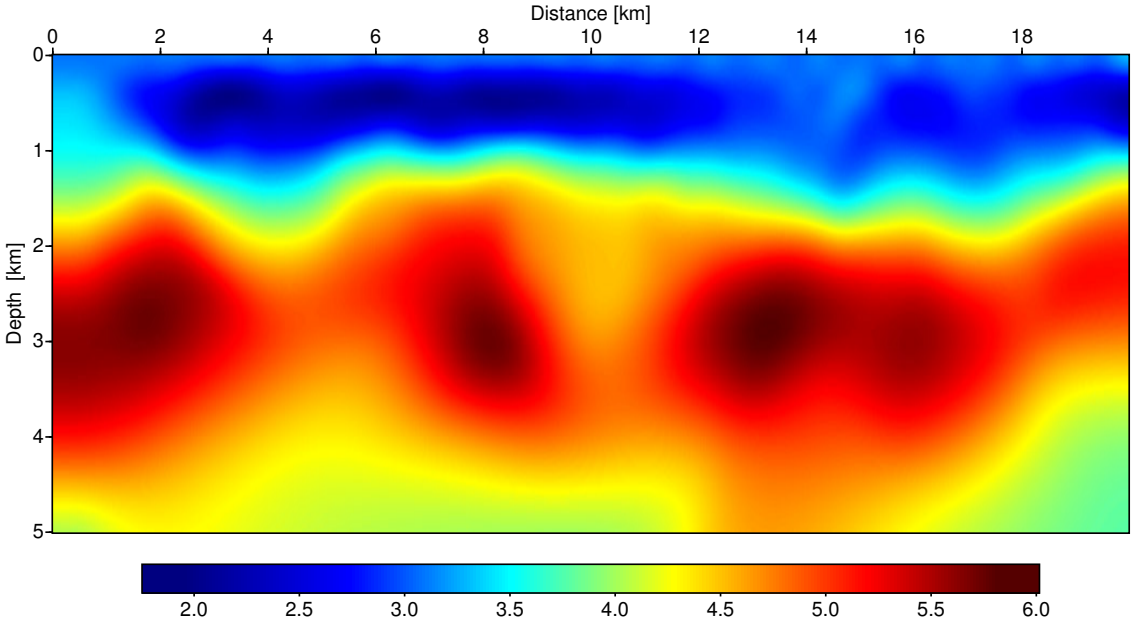

Figure 11: Macro-velocity model [km/s] obtained by CRS attribute based tomographic inversion.

offset reflection response of a common-reflection-point (CRP) in the subsurface. Therefore, the NIP wave focuses at zero traveltime at the NIP if propagated into the subsurface in a correct model. This principle can be utilized in an inversion that uses the above mentioned attributes picked in the CRS-stacked section to obtain a laterally inhomogeneous velocity model. The CRS-stack-based velocity model determination approach is realized as a tomographic inversion (Duveneck, 2004), in which the misfit between picked and forward-modeled attributes is iteratively minimized in the least-squares sense. Fortunately, the tomographic inversion has not to consider the real topography, as the redatuming procedure of the CRS stack provides stack and attribute sections related to a planar reference level.
In this case study, about 1000 ZO samples together with the associated attribute values were picked for each profile to achieve an appropriate resolution and reliability. Automatic picking was performed using a module based on the coherence associated with the ZO samples. The picked data was checked using several criteria, in order to discriminate outliers and attributes related to multiples, before the tomographic inversion process was applied. The obtained macrovelocity model is defined by 800 B-spline knots. It is displayed in Figure 11.

DEPTH MIGRATION

A Kirchhoff type prestack depth migration (PreSDM) procedure for migration from topography (Hertweck and Jäger, 2002; Jäger et al., 2003) was applied. Therefore we used the prestack data after residual static correction together with the macrovelocity model obtained by the tomographic inversion (Figure 11). The necessary kinematic Green's function tables were calculated by means of an eikonal solver. The resulting depth-migrated prestack data was firstly muted to avoid excessive pulse stretch for shallow reflectors and then stacked in offset direction in order to obtain the depth-migrated image displayed in Figure 12. Some common-image gathers (CIGs) are displayed in Figure 14, where the muting can directly be seen. As most of the events in the CIGs are flat, we can state that the estimated macrovelocity model is kinematically consistent with the data. Note that no velocity model refinement was applied after the PreSDM.

As a complementary or alternative step of the CRS-stack based imaging workflow, poststack depth migration (PostSDM) was performed. Input for the PostSDM were the final CRS-stacked section after redatuming (Figure 10) and the macrovelocity model derived from the CRS attributes (Figure 11). The result is depicted in Figure 13.

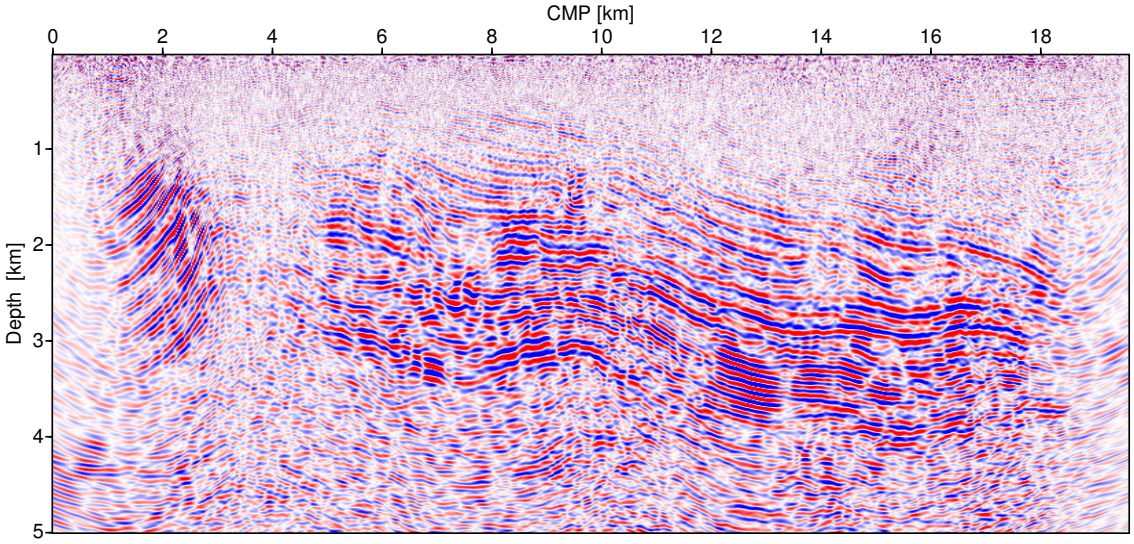

Figure 12: Prestack depth migration result.

The PostSDM result as well as the PreSDM result shows many structural details; in particular, faults, vertical offsets of reflectors, deflection of reflectors, changes of reflector characteristics across faults, and fracturing are directly observable in the sections. Although the PreSDM seems to provide a higher resolution and more details, there are also regions, especially in the deeper part, where some structures are better resolved in the PostSDM. Consequently, the PostSDM result provides complementary information and both migrated sections were used for a structural interpretation.

CONCLUSIONS

We presented results of CRS-stack-based time-to-depth imaging applied to a challenging land-data set. The work was conducted within the framework of an ongoing basin-reevaluation project. The high quality of the obtained results proves the great potential of CRS-stack-based imaging in complex land-data processing. Due to the fact that the spatial CRS stacking operator fits the searched-for reflection events in the prestack data much better than, e.g., the NMO/DMO operator an excellent signal-to-noise ratio can be achieved. Furthermore, the large fold of the CRS operator provides a significantly increased statistical basis for residual static correction making this process more precise and stable. For both, stack and residual static correction, no datum static correction of the prestack data is necessary as the topography is directly considered. A cascaded strategy for stacking and attribute extraction was presented combining two different approaches of topography handling to a very efficient implementation. The obtained CRS attributes can be used to redatum the CRS stack results so that a standardized input for further processing steps is provided. Finally, a smooth macrovelocity model well suited for subsequent depth migration is determined from the CRS attributes by means of tomographic inversion. In this way a consistent and fully data-driven imaging workflow can be established leading from time to depth domain.

The geological interpretation should be carried out mainly on the basis of Figures 10, 11, 12, and 13. Doing this, thinning , a long anticline and different faults can be mapped where plays of horsts, grabens and rollovers can be indicated. The quality of the Takutu seismic data was the main limitation for imaging the selected line. Nevertheless, the obtained results provide good ground for giving continuity to the Takutu seismic data reprocessing and reinterpretation project. Our intention is to process in the course of this ongoing project also neighboring lines in order to achieve a better geological interpretation of this part of the Takutu graben. We hope that this example serves to reinforce our perspectives and intentions on research collaboration between different universities, and between university and industry. Only in this way a continuous development of seismic exploration technology and of the "human resources" needed in

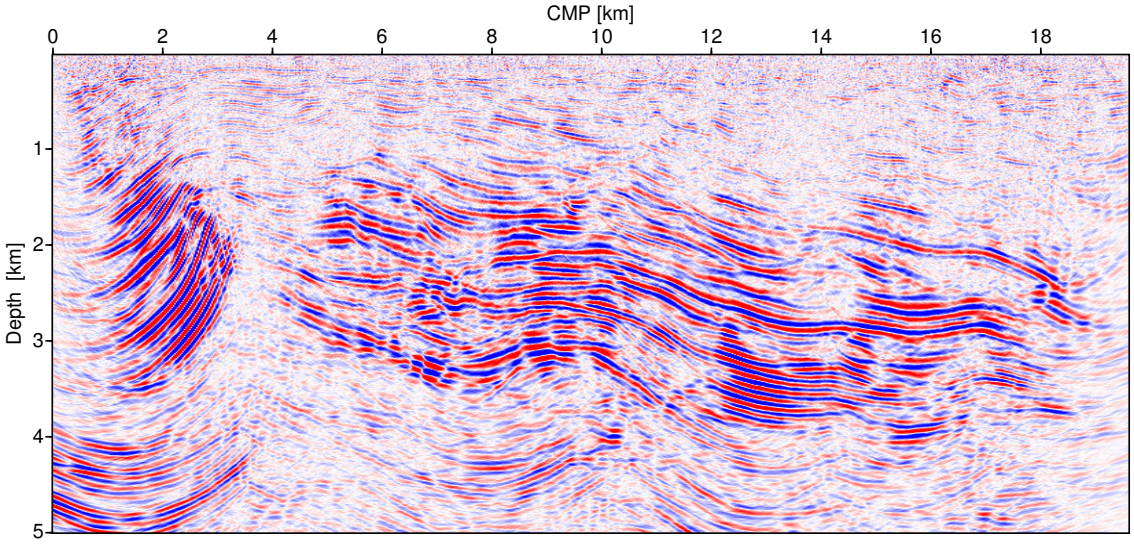

Figure 13: Poststack depth migration.

future research and production can be maintained.

ACKNOWLEDGMENTS

The authors would like to thank the Brasilian institution UFPA (Universidade Federal do Pará), FINEP (Financiadora de Estudos e Projetos), ANP (Agência Nacional do Petróleo), PETROBRAS and the project Rede Risco Exploratório (Rede 01/03, FINEP 22.01.0763.00) and the sponsors of the WIT (Wave Inversion Technology) Consortium.

REFERENCES

Bergler, S. (2001). Common-Reflection-Surface stack for common offset – theory and application. Master's thesis, Karlsruhe University.

Červený, V. (2001). *Seismic Ray Theory*. Cambridge Univ. Press, New York, 2001.

Chira, P., Tygel, M., Zhang, Y., and Hubral, P. (2001). Analytic CRS stack formula for a 2D curved measurement surface and finite-offset reflections. *Journal of Seismic Exploration*, 10(1-3):245–262.

Cohen, J. K. and Stockwell, J. J. W. (2000). Seismic Un*x Release 34: a free package for seismic research and processing. Center for Wave Phenomena, Colorado School of Mines. *Geophysical Journal International*, 125:431–442.

Duveneck, E. (2004). Velocity model estimation with data-derived wavefront attributes. *Geophysics*, 69(1):265–274.

Eiras, J. F. and Kinoshita, E. M. (1990). Geology and petroleum perspectives of the takutu basin. *In: Raja Gabaglia, G.P. and Milani, E.J. Origen and Evolution of Sedimentary Basins. (In Portuguese)*, pages 97–220.

Gierse, G., Pruessmann, J., Laggiard, E., Boennemann, C., and Meyer, H. (2003). Improved imaging of 3D marine seismic data from offshore Costa Rica with CRS processing. *First Break*, 21(12):45–49.

Gurevich, B., Keydar, S., and Landa, E. (2001). Multifocusing imaging over an irregular topography. *Geophysics*, 67(2):639–643.

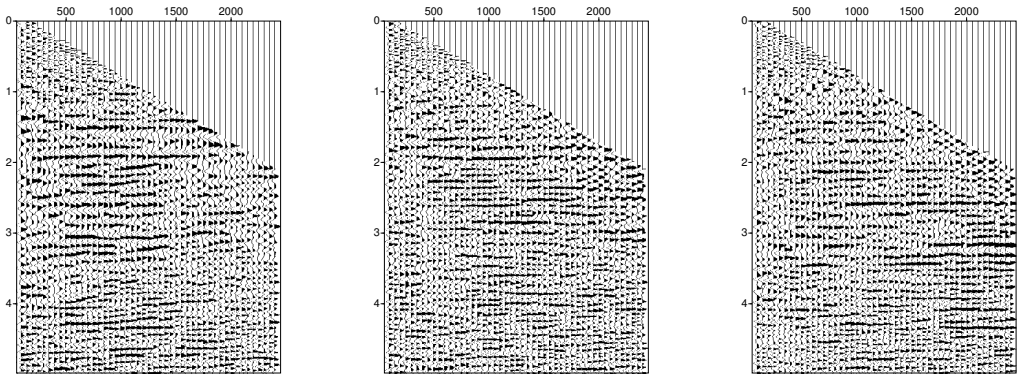

(a) CIG at $x = 2.5$ km **(b)** CIG at $x = 5.5$ km **(c)** CIG at $x = 8.5$ km

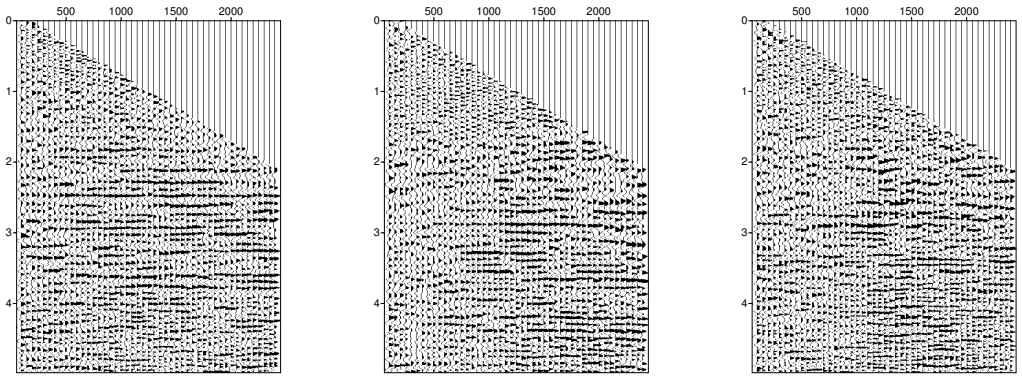

(d) CIG at $x = 11.5$ km **(e)** CIG at $x = 14.5$ km **(f)** CIG at $x = 17.5$ km

Figure 14: Some common-image gathers (CIGs) extracted from the prestack depth migration result before stacking over all offsets.

Heilmann, Z. (2003). Extensions of the Common-Reflection-Surface Stack Considering the Surface Topography and the Near-Surface Velocity Gradient. In *Ext. Abstr., 8th International Congress, Soc. Bras. Geofísica (SBGf), Rio de Janeiro*.

Hertweck, T. and Jäger, C. (2002). Short note: various aspects of Kirchhoff migration. *Annual WIT report*, pages 133–142.

Höcht, G. (1998). Common-Reflection-Surface stack. Master's thesis, Karlsruhe University.

Hubral, P. (1983). Computing true amplitude reflections in a laterally inhomogeneous earth. *Geophysics*, 48(8):1051–1062.

Hubral, P., editor (1999). *Special Issue on Macro-Model Independent Seismic Reflection Imaging*, volume 42(3,4) of *Journal of Applied Geophysics*, Amsterdam. Elsevier.

Hubral, P. and Krey, T. (1980). *Interval velocities from seismic reflection traveltime measurements*. Soc. Expl. Geophys.

Jäger, C., Hertweck, T., and Spinner, M. (2003). True-amplitude Kirchhoff migration from topography. In *Extended Abstracts*, Session MIG 2.1. 73rd Ann. Internat. Mtg., Soc. Expl. Geophys.

Jäger, R. (1999). The Common-Reflection-Surface stack – theory and application. Master's thesis, Karlsruhe University.

Jäger, R., Mann, J., Höcht, G., and Hubral, P. (2001). Common-reflection-surface stack: Image and attributes. *Geophysics*, 66:97–109.

Koglin, I. (2005). *Estimation of Residual Static Time Shifts by means of the CRS-based Residual Static Correction Approach*. Logos Verlag, Berlin.

Mann, J. (2002). *Extensions and applications of the Common-Reflection-Surface stack method*. Logos Verlag, Berlin.

Mann, J. and Duveneck, E. (2004). Event-consistent smoothing in generalized high-density velocity analysis. In *Extended Abstracts*, Session: ST1.1. 74th Annual Internat. Mtg., Soc. Expl. Geophys.

Müller, T. (1999). *The Common-Reflection-Surface stack method – seismic imaging without explicit knowledge of the velocity model*. Der andere Verlag, Bad Iburg.

Neidell, N. S. and Taner, M. T. (1971). Semblance and other coherency measures for multichannel data. *Geophysics*, 36(3):482–497.

Ronen, J. and Claerbout, J. F. (1985). Surface-consistent residual statics estimation by stack-power maximization. *Geophysics*, 50(12):2759 – 2767.

Ursin, B. (1982). Quadratic wavefront and traveltime approximations in inhomogeneous layered media with curved interfaces. *Geophysics*, 47(7):1012–1021.

von Steht, M. (2004). The Common-Reflection-Surface Stack under Consideration of the Acquisition Surface Topography – Combined Approach and Data Examples. Master's thesis, Karlsruhe University, http://www-gpi.physik.uni-karlsruhe.de/pub/wit/Downloads/diplthesis-mvsteht.pdf.

Yilmaz, Ö. (2001). *Seismic Data Analysis, Vols. 1 and 2*. Soc. Expl. Geophys.

Zhang, Y. (2003). *Common-Reflection-Surface Stack and the Handling of Top Surface Topography*. Logos Verlag, Berlin.

APPENDIX A

Based on the ray-theoretical foundations presented in Červený (2001), Zhang (2003) derived a very general CRS stacking operator for arbitrary top-surface topography. This stacking operator describes the second-order traveltime moveout along any ray in the paraxial vicinity of a chosen *central ray* by means of physically interpretable properties. These properties, called kinematic wavefield attributes, are directly related to the central ray. For comparison, in case of the well known common-midpoint (CMP) stack we have only one kinematic wavefield attribute, i. e., the stacking velocity. For the specific geometry of CMP experiments on a planar measurement surface this single parameter is sufficient to describe the traveltime moveout with offset up to the second order. In contrast to this, the CRS stack operator also takes neighboring CMP gathers into account, i. e., it describes the traveltime moveout with offset and midpoint dislocation.

In case of the zero-offset CRS stack, we choose the central ray to have the coincident source and receiver location X_0 and normal incidence on the reflecting interface. If we denote the traveltime along a paraxial

ray by t and the traveltime along the central ray by t_0, the so-called parabolic CRS stacking operator for arbitrary topography reads

$$\begin{aligned} t_{\mathrm{par}}(\Delta\vec{m},\vec{h}) &= t_0 - \frac{2}{v_0}\,(\Delta m_x \sin\beta_0 + \Delta m_z \cos\beta_0) \\ &+ \frac{K_{\mathrm{N}}}{v_0}\,(\Delta m_x \cos\beta_0 - \Delta m_z \sin\beta_0)^2 \\ &+ \frac{K_{\mathrm{NIP}}}{v_0}\,(h_x \cos\beta_0 - h_z \sin\beta_0)^2\ , \end{aligned} \tag{1}$$

where $(\Delta m_x, \Delta m_z)$ and (h_x, h_z) are the components of midpoint displacement $\Delta\vec{m} = \vec{m} - O\vec{X}_0$ and half-offset $\vec{h}$ of the considered paraxial ray. The searched-for CRS attributes are:

1. β_0, the emergence angle of the central ray measured with respect to the z-axis,
2. K_{NIP}, the curvature of the *normal-incidence-point wavefront*, and
3. K_{N}, the curvature of the *normal wavefront*.

The mentioned wavefronts are related to hypothetical eigenwaves firstly introduced by Hubral (1983). The parameter v_0 defines the near-surface velocity and is assumed to be known. By taking the square on both sides of equation (1) and keeping only terms up to second order, we obtain the hyperbolic representation,

$$\begin{aligned} t^2_{\mathrm{hyp}}(\Delta\vec{m},\vec{h}) &= \left(t_0 - \frac{2}{v_0}\,(\Delta m_x \sin\beta_0 + \Delta m_z \cos\beta_0)\right)^2 \\ &+ \frac{2\,t_0\,K_{\mathrm{N}}}{v_0}\,(\Delta m_x \cos\beta_0 - \Delta m_z \sin\beta_0)^2 \\ &+ \frac{2\,t_0\,K_{\mathrm{NIP}}}{v_0}\,(h_x \cos\beta_0 - h_z \sin\beta_0)^2\ . \end{aligned} \tag{2}$$

After systematic investigations, Ursin (1982) suggested that in most cases a hyperbolic traveltime formula is a better approximation to the real traveltime response than a parabolic one. This was later verified by the work of Höcht (1998), Müller (1999), Jäger (1999), and Bergler (2001). Therefore, we use the hyperbolic traveltime expansion for our current implementation.

Even though equations (1) and (2) are quite compact and provide an accurate and very natural description of the topography, the computational cost connected with their practical evaluation are very high. In order to determine the optimal stacking operator for a certain sample in the zero-offset section, a simultaneous search for at least two of the three CRS attributes is required. Therefore, we use equation (2) only for the local optimization of the initial attributes, determined by means of a traveltime approximation which is less accurate but better suited for a global search. Such a traveltime approximation was presented by Chira et al. (2001). We will rederive this formula in the following starting from equation (1). For this purpose, we establish in every point X_0 a local Cartesian coordinate system as depicted in Figure 15, with its origin in X_0 and its $\hat{x}$-axis being tangent to the surface in X_0. In the local coordinate system the $\hat{z}$-component of any source or receiver point in the vicinity of X_0 can be approximated up to the second order by the relation

$$\hat{z}(\hat{x}) = -\frac{K_0}{2}\hat{x}^2\ , \quad \text{with} \quad K_0 = -\frac{d^2\hat{z}}{d\hat{x}^2}\Big|_{X_0} \tag{3}$$

being the local curvature of the measurement surface in X_0. Thus, in the local coordinate system the location of two points S and G in the vicinity of X_0 reads

$$\begin{pmatrix} \hat{x}(S) \\ \hat{z}(S) \end{pmatrix} = \begin{pmatrix} m_{\hat{x}} - h_{\hat{x}} \\ -\frac{K_0}{2}(m_{\hat{x}} - h_{\hat{x}})^2 \end{pmatrix} \quad \text{and} \quad \begin{pmatrix} \hat{x}(G) \\ \hat{z}(G) \end{pmatrix} = \begin{pmatrix} m_{\hat{x}} + h_{\hat{x}} \\ -\frac{K_0}{2}(m_{\hat{x}} + h_{\hat{x}})^2 \end{pmatrix}. \tag{4}$$

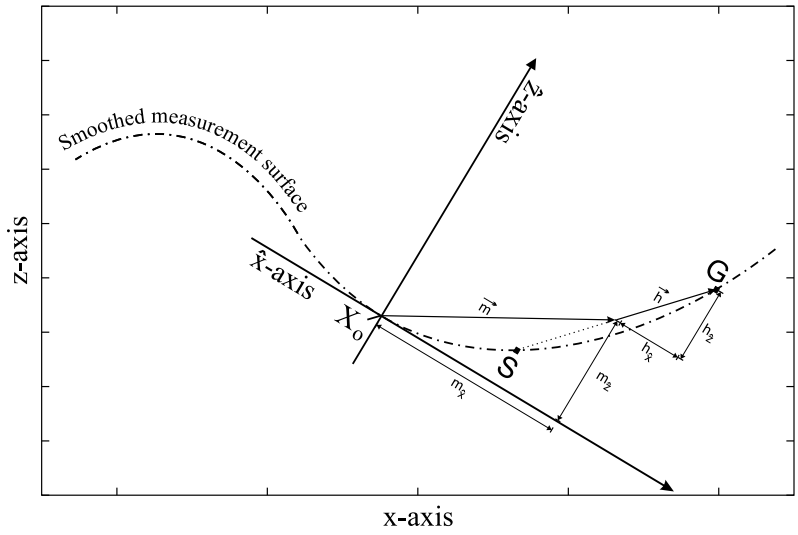

Figure 15: *Local Cartesian coordinate system with origin in X_0 and $\hat{x}$-axis tangent to the measurement surface in X_0.*

For the corresponding midpoint and half-offset vectors we find, according to Figure 15,

$$\vec{m}(S,G) = \begin{pmatrix} m_{\hat{x}} \\ m_{\hat{z}} \end{pmatrix} = \tfrac{1}{2} \begin{pmatrix} \hat{x}(G) + \hat{x}(S) \\ \hat{z}(G) + \hat{z}(S) \end{pmatrix} = \begin{pmatrix} m_{\hat{x}} \\ -\frac{K_0}{2}(m_{\hat{x}}^2 + h_{\hat{x}}^2) \end{pmatrix} , \tag{5}$$

$$\vec{h}(S,G) = \begin{pmatrix} h_{\hat{x}} \\ h_{\hat{z}} \end{pmatrix} = \tfrac{1}{2} \begin{pmatrix} \hat{x}(G) - \hat{x}(S) \\ \hat{z}(G) - \hat{z}(S) \end{pmatrix} = \begin{pmatrix} h_{\hat{x}} \\ -K_0 m_{\hat{x}} h_{\hat{x}} \end{pmatrix} . \tag{6}$$

Denoting the dip angle of the measurement surface in X_0 with respect to a global z-axis by α_0 we obtain for Δm_z and h_z after a simple rotation of the coordinate system

$$\Delta m_x = m_{\hat{x}} \cos\alpha_0 - m_{\hat{z}} \sin\alpha_0 , \qquad h_x = h_{\hat{x}} \cos\alpha_0 - h_{\hat{z}} \sin\alpha_0 , \tag{7}$$

$$\Delta m_z = m_{\hat{x}} \sin\alpha_0 + m_{\hat{z}} \cos\alpha_0 , \qquad h_z = h_{\hat{x}} \sin\alpha_0 + h_{\hat{z}} \cos\alpha_0 . \tag{8}$$

From equations (5), (6), and (7) we can derive

$$m_{\hat{x}} = \frac{\Delta m_x}{\cos\alpha_0} - \frac{\sin\alpha_0}{\cos\alpha_0}\frac{K_0}{2}(m_{\hat{x}}^2 + h_{\hat{x}}^2) \quad \text{and} \quad h_{\hat{x}} = \frac{h_x}{\cos\alpha_0} - \frac{\sin\alpha_0}{\cos\alpha_0} K_0 m_{\hat{x}} h_{\hat{x}}. \tag{9}$$

Multiplying the above equations by $m_{\hat{x}}$ and $h_{\hat{x}}$, respectively, we find the second order approximation

$$m_{\hat{x}}^2 = \frac{\Delta m_x^2}{\cos^2\alpha_0} , \qquad h_{\hat{x}}^2 = \frac{h_x^2}{\cos^2\alpha_0} , \quad \text{and} \quad m_{\hat{x}} h_{\hat{x}} = \frac{\Delta m_x h_x}{\cos^2\alpha_0} . \tag{10}$$

Together with equations (5), (6), (8) and (9), this leads to the following expressions

$$\Delta m_z = \frac{\sin\alpha_0 \Delta m_x}{\cos\alpha_0} - \frac{K_0}{2\cos^3\alpha_0}(\Delta m_x^2 + h_x^2) , \tag{11}$$

$$h_z = \frac{\sin\alpha_0 h_x}{\cos\alpha_0} - \frac{K_0}{\cos^3\alpha_0}\Delta m_x h_x . \tag{12}$$

Inserting equations (11) and (12) into equation (1) and retaining only terms up to the second order yields the parabolic CRS traveltime operator for smoothly curved topography. By squaring both sides and keeping again only terms up to second order, we obtain the hyperbolic CRS traveltime operator for smooth curved

topography:

$$\begin{aligned} t^2_{\mathrm{hyp}}(\Delta m_x, h_x) &= \left(t_0 + \frac{2\,\Delta m_x}{v_0\,\cos\alpha_0}\,\sin(\beta_0+\alpha_0)\right)^2 \\ &+ \frac{2\,t_0\,\Delta m_x^2}{v_0\,\cos^2\alpha_0}\,\left(K_{\mathrm{N}}\,\cos^2(\beta_0+\alpha_0) - K_0\,\cos(\beta_0+\alpha_0)\right) \\ &+ \frac{2\,t_0\,h_x^2}{v_0\,\cos^2\alpha_0}\,\left(K_{\mathrm{NIP}}\,\cos^2(\beta_0+\alpha_0) - K_0\,\cos(\beta_0+\alpha_0)\right)\,. \end{aligned} \tag{13}$$

Setting $K_0 = 0$ and $\alpha_0 = 0$ the above traveltime operator reduces to the well-known zero-offset CRS stack formula for a planar measurement surface (see, e. g. Höcht, 1998; Müller, 1999; Mann, 2002). For convenience this formula (in different notation) is repeated here. It reads

$$\begin{aligned} t^2_{\mathrm{hyp,planar}}(\Delta m_x, h_x) &= \left(t_0 + \frac{2}{v_0}\,\Delta m_x\,\sin\beta_0\right)^2 \\ &+ \frac{2\,t_0}{v_0}\,K_{\mathrm{N}}\,\cos^2\beta_0\,\Delta m_x^2 \\ &+ \frac{2\,t_0}{v_0}\,K_{\mathrm{NIP}}\,\cos^2\beta_0\,h_x^2\,. \end{aligned} \tag{14}$$

APPENDIX B

The redatuming of the zero-offset samples of stack and attribute sections is composed of a lateral displacement Δx and a time shift Δt. Denoting the emergence point of the zero-offset ray at the planar reference level by $X'_0(x'_0, z'_0)$ the respective transformations read

$$x'_0 = x_0 + \Delta x = x_0 + (z'_0 - z_0)\,\tan\beta_0 \quad \text{and} \quad t'_0 = t_0 + \Delta t = t_0 + \frac{2\,(z'_0 - z_0)}{v_0\,\cos\beta_0}\,. \tag{15}$$

An important aspect to be considered by the redatuming procedure is that the stack amplitudes and especially the CRS attributes K_{NIP} and K_{N} alter their values while the zero-offset ray is continued. The *propagation law* (see, e. g., Hubral and Krey, 1980) yields for the two wavefront radii K'_{NIP} and K'_{N} measured at the planar reference level

$$K'_{\mathrm{NIP}} = \left(\frac{1}{K_{\mathrm{NIP}}} + \frac{1}{2}\,\Delta t\,v_0\right)^{-1} \quad \text{and} \quad K'_{\mathrm{N}} = \left(\frac{1}{K_{\mathrm{N}}} + \frac{1}{2}\,\Delta t\,v_0\right)^{-1} \tag{16}$$

The values of the emergence angle are not altered by the redatuming as no refraction occurs at the smoothly curved reference level due to the condition $v_r = v_0$. To map the stack amplitudes, the *geometrical spreading factor* calculated from the CRS attributes could be used to extrapolate appropriate values corresponding to the planar reference level. However, this is not yet implemented and the amplitudes are currently mapped without altering their values.